Elucidating the role of *Agl* in bladder carcinogenesis by generation and characterization of genetically engineered mice

Joseph L.Sottnik[1,†], Vandana Mallaredy[1,†], Ana Chauca-Diaz[1], Carolyn Ritterson Lew[1], Charles Owens[1], Garrett M. Dancik[2], Serena Pagliarani[3], Sabrina Lucchiari[3], Maurizio Moggio[3], Michela Ripolone[3], Giacomo P.Comi[4], Henry F.Frierson Jr[5], David Clouthier[6] and Dan Theodorescu[1,7,*]

[1]Department of Surgery, University of Colorado–Anschutz Medical Campus, Aurora, CO 80045, USA, [2]Department of Computer Science, Eastern Connecticut State University, Willimantic, CT 06226, USA, [3]Neuromuscular and Rare Diseases Unit, Department of Neuroscience and Mental Health, Fondazione IRCCS Ca' Granda Ospedale Maggiore Policlinico, Milan, Italy, [4]Department of Pathophysiology and Transplantation, University of Milan, and Neurology Unit, Fondazione IRCCS Ca' Granda Ospedale Maggiore Policlinico, Milan, Italy, [5]Department of Pathology, University of Virginia, Charlottesville, VA 22908, USA, [6]Department of Craniofacial Biology and [7]Samuel Oschin Comprehensive Cancer Institute, Los Angeles, CA 90048, USA

*To whom correspondence should be addressed. Tel: +1 310 4238431; Fax: 1-310-423-8300; Email: dan.theodorescu@cshs.org
†These authors contributed equally to this work.

Abstract

Amylo-α-1,6-glucosidase,4-α-glucanotransferase (AGL) is an enzyme primarily responsible for glycogen debranching. Germline mutations lead to glycogen storage disease type III (GSDIII). We recently found AGL to be a tumor suppressor in xenograft models of human bladder cancer (BC) and low levels of AGL expression in BC are associated with poor patient prognosis. However, the impact of low AGL expression on the susceptibility of normal bladder to carcinogenesis is unknown. We address this gap by developing a germline *Agl* knockout ($Agl^{-/-}$) mouse that recapitulates biochemical and histological features of GSDIII. $Agl^{-/-}$ mice exposed to *N*-butyl-*N*-(4-hydroxybutyl) nitrosamine (BBN) had a higher BC incidence compared with wild-type mice ($Agl^{+/+}$). To determine if the increased BC incidence observed was due to decreased *Agl* expression in the urothelium specifically, we developed a urothelium-specific conditional *Agl* knockout (Agl^{cko}) mouse using a Uroplakin II-Cre allele. BBN-induced carcinogenesis experiments repeated in Agl^{cko} mice revealed that Agl^{cko} mice had a higher BC incidence than control ($Agl^{fl/fl}$) mice. RNA sequencing revealed that tumors from $Agl^{-/-}$ mice had 19 differentially expressed genes compared with control mice. An '*Agl* Loss' gene signature was developed and found to successfully stratify normal and tumor samples in two BC patient datasets. These results support the role of AGL loss in promoting carcinogenesis and provide a rationale for evaluating *Agl* expression levels, or *Agl* Loss gene signature scores, in normal urothelium of populations at risk of BC development such as older male smokers.

Introduction

Bladder cancer (BC) is expected to occur in approximately 81 000 patients in 2018, making it the fifth most common cancer in the USA (1). We have previously identified amylo-α-1,6-glucosidase, 4-α-glucanotransferase (AGL) as a tumor suppressor in BC, with decreased AGL expression associated with increased tumor aggressiveness (2,3). AGL is a metabolic enzyme primarily responsible for glycogen debranching (4). Interestingly, we have shown that the canonical role of AGL, glycogen debranching, is

Abbreviations

AGL	amylo-α-1,6-glucosidase,4-α-glucanotransferase
BBN	N-butyl-N-(4-hydroxybutyl) nitrosamine
BC	bladder cancer
GDE	glycogen debranching enzyme
GDF15	Growth differentiation factor 15
GSDIII	glycogen storage disease type III
ITGB4	integrin subunit beta 4
qPCR	quantitative real-time PCR
RNA-seq	RNA sequencing
UPKII	Uroplakin II

not implicated in regulating tumor growth (2). Our investigations into the mechanisms underlying this noncanonical function have shown that increased growth and metastasis is related to increased expression of hyaluronic acid synthase 2 HAS2 secondary to AGL loss (3). Hyaluronic acid synthase 2 (HAS2) in turn leads to increased expression and secretion of hyaluronic acid that activates its receptors, CD44 and the hyaluronan-mediated motility receptor RHAMM and in this way promotes aggressive tumor behavior (5–7).

In addition to progressively lower AGL levels being associated with increased tumor aggressiveness, AGL expression is lower in tumors when compared with normal urothelium. These observations suggest that reduced AGL expression is permissive for bladder tumor formation. In humans, inactivating germline mutations of *AGL* have been observed and result in glycogen storage disease type III (GSDIII) (7–10). However, epidemiological studies examining whether GSDIII patients have a higher risk of developing BC are difficult because (i) the number of patients is small, (ii) most patients in international registries are relatively young and (iii) there is a low smoking prevalence. The latter two factors, age and tobacco use, are major risk factors for BC development (8,11).

Given the inability to address this clinical question with epidemiological studies, we sought to develop novel murine models to address the gap in the literature regarding the role of AGL in malignant transformation of bladder urothelium. Herein, we describe a conventional germline *Agl* knockout mouse and use it to investigate *N*-butyl-*N*-(4-hydroxybutyl) nitrosamine (BBN)-induced bladder carcinogenesis. BBN is a common way to induce experimental BC and has been shown to mimic human disease development and molecular characteristics (12). To determine if the effects are due to lack of *Agl* specifically in the urothelium, we developed a conditional knockout model based on the Cre/LoxP system, in which *Cre* expression driven by the Uroplakin II (UpkII) promoter leads to the specific loss of *Agl* in the urothelium (13). Using these models, we show that *Agl* deletion increases the incidence of BC, supporting its role as a suppressor of transformation.

Materials and methods

Animal use and repository

All animal studies were performed in an AAALAC-approved facility with the approval of the University of Colorado–Denver Institutional Animal Care and Use Committee (IACUC). Animals are available to the scientific community from the Gates Bioengineering Core at the University of Colorado–Denver.

Development of conventional germline *Agl* knockout (*Agl*$^{-/-}$) mice

A conventional germline *Agl* knockout mouse strain was developed by injecting JM8A3.N1 ES cells containing a targeted *Agl* locus [Agl$^{tm1e(EUCOMM)Wtsi}$ vector; European Conditional Mouse Mutagenesis (EUCOMM) program] into blastocysts, which were subsequently implanted in pseudopregnant females. Resulting founder mice were genotyped using primers developed by EUCOMM, with expansion of positive animals resulting in the establishment of a targeted *Agl*^{tm1e} strain; hereafter referred to as *Agl*$^{+/-}$. Although no exons were deleted in the tm1e allele, the allele is classified as a targeted, nonconditional knockout allele due to the preferential splicing that occurs with the En2-SA portion of the construct leading to a premature stop site incorporated after exon 5. A similar targeting strategy has been previously used to disrupt *Agl* (14). Heterozygous mice were intercrossed to produce *Agl*$^{-/-}$ mice. *Agl*$^{+/+}$ mice were used as controls. Genotyping of 3-week old mice was performed from tail snips. DNA was isolated using the Qiagen DNAeasy Blood and Tissue kit (Valencia, CA). PCR was performed using GoTaq Green Master Mix (Promega, Madison, WI) with 0.4 μM PCR primers (Supplementary Table I). PCR products were visualized on 1% ethidium bromide agarose gels using a Bio-Rad ChemiDoc MP Imaging System (Hercules, CA). The wild-type *Agl* allele (*Agl*$^{+/+}$) produces a PCR product of 522 bp whereas the *Agl*$^{-/-}$ allele produces a product of 395 bp. To verify systemic loss of *AGL* protein expression, a western blot of liver tissue was performed. Briefly, liver was homogenized in RIPA lysis buffer and quantified by BCA kit (Thermo Scientific, Rockford, IL). Samples were run on a 4–20% Tris-glycine gel (Thermo Scientific), transferred to polyvinylidene difluoride, blocked in 5% nonfat dry milk and probed with rabbit polyclonal anti-AGL (Agrisera, Vännäs, Sweden) and mouse monoclonal anti-tubulin (Developmental Studies Hybridoma Bank, University of Iowa, Iowa City, IA) overnight. Blots were imaged using a Bio-Rad ChemiDoc MP Imaging System.

Development of urothelium-specific *Agl* conditional knockout (*Agl*^{cko}) mice

Derivation of an urothelium-specific conditional knockout mouse strain (*Agl*^{cko}) was achieved through *in vitro* fertilization using sperm (B6NTac;B6N-*Agl*$^{tm1a(EUCOMM)Wtsi}$) from EUCOMM and wild-type C57BL/6J oocytes. Fertilized ova were transferred at the two-cell stage into pseudopregnant female recipients as described previously (15). Resulting *Agl*^{tm1a} mice were then mated with mice from the FLPo deleter strain 129S4/SvJaeSor-*Gt(ROSA)26Sor*$^{tm1(FLP1)Dym}$/J (The Jackson Laboratory, Bar Harbor, ME) to remove the FRT sites on either side of the neomycin selection and *lacZ* cassettes, leaving only *lox*P sites flanking exons 6–10. These mice (*Agl*^{tm1c}, subsequently referred to as *Agl*$^{fl/+}$) were intercrossed to create *Agl*$^{fl/fl}$ mice. *Agl*$^{fl/fl}$ mice were then bred with Uroplakin II-Cre mice (*UpkII-Cre*$^{+/Tg}$; a generous gift from Dr. Xue-Ru Wu) (16), in which *Cre* expression is restricted to the bladder urothelium (16–18). The resulting *Agl*$^{fl/+}$;*UpkII-Cre*$^{+/Tg}$ mice were then crossed with *Agl*$^{fl/fl}$ mice to produce *Agl*$^{fl/fl}$;*UpkII-Cre*$^{+/Tg}$ mice, subsequently referred to *Agl*^{cko} mice. *Agl*$^{fl/fl}$ mice were used as controls for all experiments. Genotyping was performed as described earlier. PCR primers are described in Supplementary Table I. The presence of *Cre* is identified through a 420 bp product. The wild-type *Agl* allele produces a 522 bp PCR product whereas the *Agl*$^{fl/fl}$ allele produces a 719 bp product. Under non-recombined conditions, the distance between the primers to assess recombination is 10.6 kb, a band size not probably seen in most PCRs. *Cre*-based recombination of the *Agl*$^{fl/fl}$ allele produces an 829 bp product using the described recombination primers.

BBN carcinogenesis in genetically engineered mice

Mice were treated with 0.05% or 0.1% BBN (TCI America, Portland, OR) in drinking water per schedules shown in Figures 1 and 2. Bottles were refreshed with BBN twice weekly and mice were allowed to drink *ad libitum*. Mice were inspected weekly for any endpoint that would trigger euthanasia according to our IACUC-approved protocol. After 12 weeks, BBN was removed from the water. Mice were euthanized at the time points shown in Figures 1 and 2. Bladder, liver, skeletal muscle (rectus femoris and vastus medialis) and heart were harvested, bisected and fixed in 4% paraformaldehyde (Affymetrix, Cleveland, OH) or snap frozen in liquid nitrogen.

Glycogen biology assays

Glycogen debranching enzyme (GDE) activity was measured as described elsewhere (9,19,20). Skeletal muscle, heart and liver tissue were isolated, and analysis performed by an indirect assay based on stimulation of the incorporation of radioactive glucose into glycogen. The reaction was stopped after 5 and 10 min and the enzyme activity was measured. We evaluated GDE activity as the average of the two determinations. Enzyme

activity was expressed as picomoles of glucose incorporated into glycogen/min/mg protein. Amyloglucosidase digestion of ethanol-precipitated glycogen was used to assess tissue glycogen content. Glucose concentration was estimated after amyloglucosidase digestion with Glucose (HK) Assay Kit (Sigma–Aldrich, St. Louis, MO). Absorbance was read at 340 nm after a 15 min incubation at room temperature (9,19).

Tumor histology

Paraformaldehyde-fixed tissues were paraffin-embedded and processed for hematoxylin and eosin staining to assess size and organization of tumors. All bladders were evaluated by a board-certified pathologist in a blinded manner with respect to the mouse genotype. Histologic images were acquired using an Olympus DP27 camera (Olympus, Parkway Center Valley, PA) and Leica Aperio ImageScope software (Wetzlar, Germany).

RNA sequencing

Flash-frozen tumor samples from $Agl^{+/+}$ and $Agl^{-/-}$ mice were weighed, crushed, and RNA purified using the RNeasy Plus Mini Kit (Qiagen). RNA was subsequently sent to Novogene (Chula Vista, CA), where library preparation and RNA sequencing (RNA-seq) were performed). Differentially expressed genes were determined using Novogene's standard analysis pipeline, which includes aligning reads using TopHat2 and differential expression analysis using DESeq2 'R' package with an false discovery rate (FDR) <0.05. All relevant files were uploaded to the NCBI Gene Expression Omnibus repository (GSE113158).

Microarray analysis

For microarray analysis, gene expression datasets from two BC patient cohorts were used. The Memorial Sloan Kettering Cancer Center cohort consists of 129 samples reported by Sanchez-Carbayo *et al.* (21). The second cohort consists of 175 samples collected from the Chungbuk National University Hospital (22), with Gene Expression Omnibus accession number GSE13507 (23). For genes with multiple probes, the probe with the highest mean expression was used (24). For each probe, expression values were normalized to have a mean expression of 0 and standard deviation of 1. The '*Agl* Loss' score is the sum of normalized expression values of genes whose expression are higher in tumors of $Agl^{-/-}$ mice minus the sum of normalized expression values for genes that are lower in $Agl^{-/-}$ tumors compared with $Agl^{+/+}$ tumors. Thus, human tumors with higher scores are more like $Agl^{-/-}$ tumors than those human tumors with lower scores. The area under the receiver operating characteristics curve, fold changes and nonparametric Wilcoxon rank sum test were used to evaluate whether gene expression values for single genes or $Agl^{-/-}$ scores differed between BC and normal human urothelium samples. *P*-values of <0.05 are considered statistically significant.

Quantitative real-time PCR

RNA was prepared from flash-frozen tumor as described earlier for RNA-seq analysis and reverse transcribed using the iScript Reverse Transcription Supermix (Bio-Rad). Quantitative real-time PCR (qPCR) was performed in duplicate for each tumor using iTaq Universal SYBR Green Supermix (Bio-Rad) in a 10 µl reaction volume on a QuantStudio 6 Flex

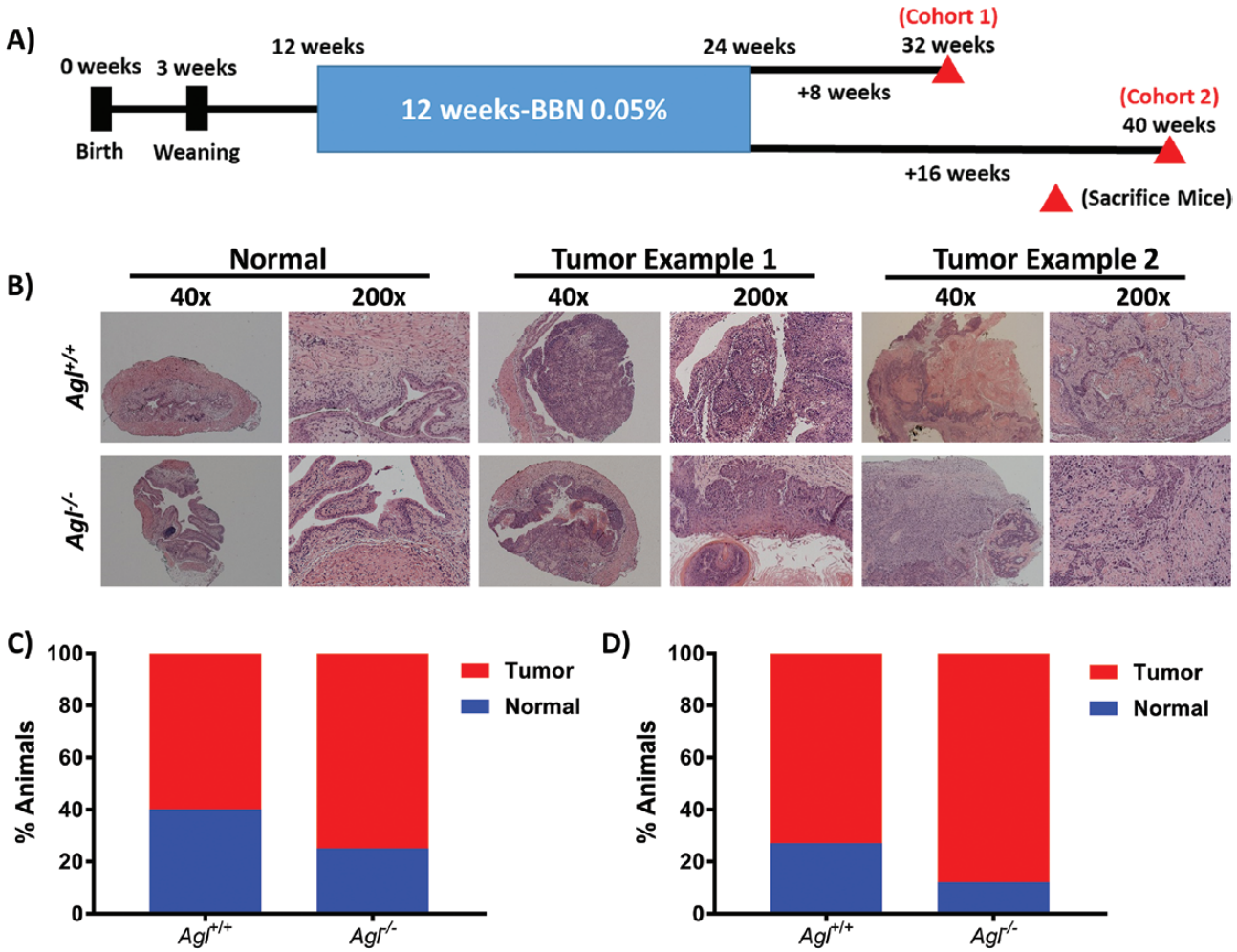

Figure 1. Incidence of BC in $Agl^{-/-}$ mice. (**A**) Overview of experimental design and two cohorts. Both cohorts were treated with 0.05% BBN for 12 weeks prior to euthanasia at 8 (cohort 1) or 16 (cohort 2) weeks after discontinuing BBN. (**B**) Representative hematoxylin and eosin images of tumor bearing bladders from $Agl^{+/+}$ and $Agl^{-/-}$ mice are shown. (**C**) $Agl^{-/-}$ mice from cohort 1 had an increased, though not statistically significant, tumor incidence compared with $Agl^{+/+}$ mice ($P > 0.05$). (**D**) $Agl^{-/-}$ mice in cohort 2 had an increased, though not statistically significant, tumor incidence compared with $Agl^{+/+}$ mice ($P > 0.05$). Fisher's exact test was used for statistical analysis.

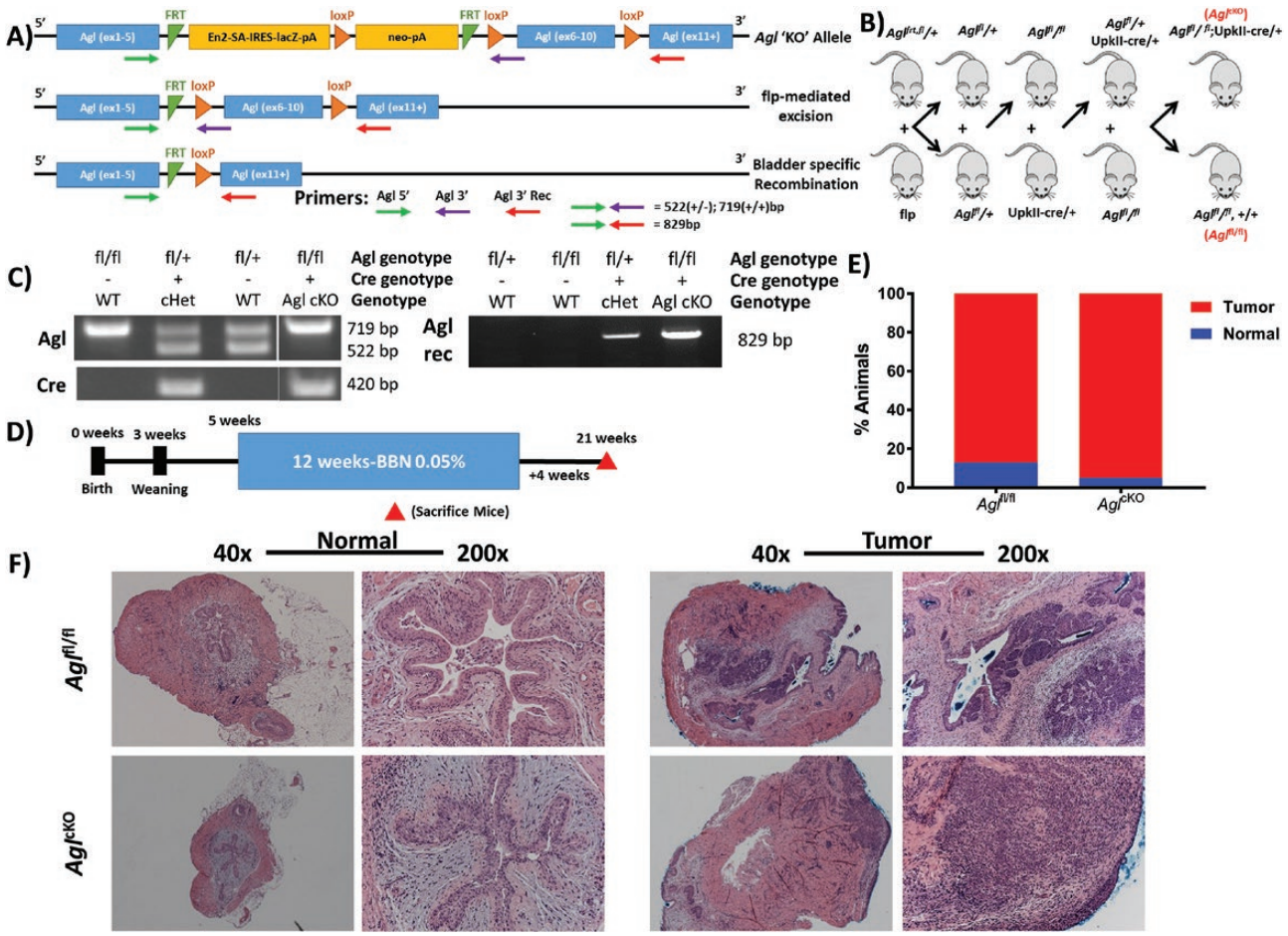

Figure 2. Incidence of BC in mice with urothelium-specific loss of *Agl*. (**A**) Diagram of the *Agl* targeting construct used to generate a urothelium-targeted allele for *Agl* knockout. FLPo-mediated excision followed by Cre recombinase-mediated recombination (by crossing with *UpkII-Cre* mice) leads to targeted deletion of *Agl* in the urothelium. Relative primer locations and amplicon sizes expected from genotyping are shown. (**B**) The breeding strategy used to develop control ($Agl^{fl/fl}$) and Agl^{cko} ($Agl^{fl/fl}$;$UpkII\text{-}Cre^{+/Tg}$) mice. (**C**) PCR genotyping of animals; the floxed *Agl* allele produces a 719 bp amplicon whereas the wild-type *Agl* allele produces a 522 bp amplicon. The presence of Cre produces a 420 bp amplicon. Cre-based *Agl* recombination was confirmed in the bladders of Agl^{cko} mice by an 829 bp recombination-specific amplicon. (**D**) Mice were treated with 0.05% BBN for 12 weeks and euthanized 4 weeks following BBN discontinuation. (**E**) Agl^{cko} mice had an increased, though not statistically significant ($P > 0.05$), incidence of tumor formation compared with $Agl^{fl/fl}$ mice. (**F**) Representative histologic analyses of $Agl^{fl/fl}$ and Agl^{cko} mice with normal bladder epithelium and invasive carcinomas are shown. Fisher's exact test was used for statistical analysis.

(Applied Biosystems, Foster City, CA). Measurements from duplicate C_t values were normalized to Fkbp5, averaged and reported using the $\Delta\Delta C_t$ method.

Statistical analysis

Statistical analyses, not previously detailed, were performed using GraphPad Prism v7 software (GraphPad Software, La Jolla, CA). Student's *t*-test and Fisher's exact tests were used to analyze carcinogenesis data. qPCR data were analyzed using ROUT to identify and remove statistical outliers followed by the Kolmogorov–Smirnov test. Power calculations, comparing two independent samples with inference for proportions with $\alpha = 0.05$, power = 0.8, two-sided test, were performed using the online calculator available at https://www.stat.ubc.ca/~rollin/stats/ssize/b2.html. Results are means ± SEM, and significance is represented by $^{*}P < 0.05$, $^{**}P < 0.01$, $^{***}P < 0.001$, and $^{****}P < 0.0001$

Results

Development of a germline *Agl* knockout ($Agl^{-/-}$) mouse model

We have shown previously that inhibition of AGL leads to enhanced tumor growth (2). However, the impact AGL loss has on the incidence of urothelial carcinogenesis has yet to be determined. Therefore, a germline (full body) *Agl* knockout mouse ($Agl^{-/-}$) strain was developed and used to determine if AGL loss changes the incidence of BC following carcinogen exposure. AGL loss was evaluated using PCR (Supplementary Figure 1A) and western blotting (Supplementary Figure 1B). Although we were developing our $Agl^{-/-}$ mice, two other groups reported genetically similar animals (9,14). Our model system uses a similar construct as described in Liu *et al.* (14), but was derived independently. We observed that our $Agl^{-/-}$ mice were fertile but produced small litters (1–2 pups), thus making large-scale experiments quite challenging. Importantly, we did not see any no histological evidence of altered bladder development or structural abnormalities in the $Agl^{-/-}$ mice we derived (Supplementary Figure 1C).

Impact of germline loss of *Agl* on BBN induction of bladder cancer in mice

To investigate the impact of germline *Agl* disruption on BC incidence, $Agl^{-/-}$ and $Agl^{+/+}$ mice were treated with 0.05% BBN for 12 weeks. BBN-treated mice were then divided into two cohorts (Figure 1A). The first group of mice (cohort 1; $Agl^{-/-}$, $n = 8$ and

$Agl^{+/+}$, n = 10) were euthanized 8 weeks after discontinuation of BBN treatment. The second group of mice (cohort 2; $Agl^{-/-}$, n = 7 and $Agl^{+/+}$, n = 11) were euthanized 16 weeks after discontinuation of BBN treatment. Bladders from all mice were isolated and histologic analysis was performed (Figure 1B). We observed that $Agl^{-/-}$ mice in both cohorts had an increased, though non-statistically significant tumor incidence compared with $Agl^{+/+}$ mice (Figure 1C and D). Because of the small litter sizes, a power calculation was performed and determined that 134 mice per group would be necessary to fully assess significant differences between these groups. The observations concerning increased tumor incidence in $Agl^{-/-}$ mice support our previous observation implicating AGL as a tumor suppressor.

$Agl^{-/-}$ mice created by other groups showed signs of glycogen storage disease similar to human GSDIII (9,14). We sought to determine if the mice we developed, and treated with 0.1% BBN, harbored similar pathologies. We found that the livers of $Agl^{-/-}$ mice treated with BBN were significantly enlarged compared with livers of $Agl^{-/-}$ mice ($P < 0.05$; Supplementary Figure 1D). Hematoxylin and eosin stained sections of liver, heart and skeletal muscle tissue from $Agl^{-/-}$ mice showed tissue architecture associated with the accumulation of glycogen in hepatocytes compared with $Agl^{+/+}$ mice (Supplementary Figure 2) similar to previous observations (9,14). These pathologies were like those described previously in other models of GSDIII (9,14,19). In addition, we measured GDE, the enzyme encoded by the *Agl* gene, activity in liver, heart and skeletal muscle. In these tissues, GDE activity was significantly decreased in $Agl^{-/-}$ mice when compared with $Agl^{+/+}$ mice ($P < 0.05$); Supplementary Figure 1E). Furthermore, glycogen content in all tissues examined was significantly increased ($P < 0.05$), due to decreased ability to debranch and mobilize glycogen (Supplementary Figure 1F). The GSDIII phenotype observed in our $Agl^{-/-}$ BBN-treated mice is retained similarly to previously published accounts in non-BBN-treated mice (9,14).

Impact of urothelium-specific loss of AGL on BBN induction of BC in mice

Germline deletion of *Agl* may lead to systemic metabolic alterations such as GSDIII. Such germline deletion may also impact BC development by altering BBN metabolism that occurs in the liver (25,26), possibly altering the carcinogenic potential of BBN. To mitigate these concerns, we developed a model of *Agl* loss specific to the bladder urothelium. Briefly, mice carrying a floxed *Agl* allele ($Agl^{fl/fl}$) (Figure 2A and B) were crossed with mice carrying a UpkII promoter-driving *Cre* expression (*UpkII-Cre*) (13). *UpkII* expression has been shown previously to be restricted to the bladder urothelium (27,28), meaning that $Agl^{fl/fl}$;*UpkII-Cre*$^{+/Tg}$ (Agl^{cko}) mice have a urothelium-specific loss of *Agl*. To confirm *Agl* recombination and functional deletion of *Agl*, a confirmatory analysis was performed on the bladders of a cohort of mice. Indeed, the presence of an 829 bp amplicon confirms the Cre-based recombination of *Agl* specific to the bladder (Figure 2C). PCR validation was necessary due to the lack of an adequate antibody for immunohistochemistry despite our best efforts to perfect this technique (data not shown). To investigate the impact of urothelium-specific loss of *Agl* on BC incidence, mice ($Agl^{fl/fl}$, n = 17 and Agl^{cko}, n = 18) were treated with 0.05% BBN for 12 weeks and then euthanized 4 weeks after discontinuing BBN treatment (Figure 2D). A power calculation determined that 200 mice per group would be necessary to fully assess significant differences between these groups. Histologic analysis of bladder tissue showed an increased, though not statistically significant, tumor incidence in Agl^{cko} mice when compared with $Agl^{fl/fl}$ mice (Figure 2E). A wide variety of tumor sizes were observed in both groups, with some tumors only measureable microscopically whereas others were observed to be large and invasive (Figure 2F). As for the germline deletion mouse, these observations further support our previous observation that AGL is a tumor suppressor.

RNA sequencing analysis of bladder tumors from wild-type and germline *Agl*-deleted mice

To begin our understanding of the mechanism by which *Agl* loss leads to a greater susceptibility to BBN-induced BC, tumors were isolated from $Agl^{+/+}$ and $Agl^{-/-}$ mice (n = 4 per group) and prepared for RNA-seq. Tumors from $Agl^{+/+}$ and $Agl^{-/-}$ mice were used because of the cleaner biological system afforded by the germline *Agl* deletion compared with tumors from Agl^{cko} mice. In Agl^{cko} mice, *Agl* expression from the tumor-associated stroma and immune infiltrate would potentially confound the results as *Agl* would be expressed from all cells outside the urothelium. Furthermore, because GSDIII is rare, our $Agl^{-/-}$ mouse model is perhaps the most practical approach to study tumor predisposition in these patients as discussed earlier.

Unsupervised hierarchical clustering of the eight tumor samples significantly differentiated $Agl^{+/+}$ and $Agl^{-/-}$ tumor samples (Figure 3A), with six genes significantly downregulated and 13 genes significantly upregulated (FDR < 0.05) in $Agl^{-/-}$ mice (Figure 3B; Supplementary Table II). *Agl* was identified as one of the genes significantly ($P < 0.05$) downregulated in $Agl^{-/-}$ tumors, and was validated by qPCR (Supplementary Figure 3), further validating the knockout model. To determine the global biological relevance of these genes, we developed an *Agl* Loss gene signature score. We sought to determine if normal urothelial samples and tumor tissue from patients with BC had different *Agl* Loss scores. Using data from two publicly available patient datasets, where both tumor tissue and normal tissue were available (CNUH and MSKCC (21,22)), we found that the '*Agl* Loss' score was significantly ($P < 0.05$) higher in tumor than normal tissue (Figure 3C), supporting the notion that AGL loss plays a role in BC formation. Single gene analysis of the 19 genes identified by RNA-seq was then performed to identify genes with significant relationships and directionalities to those identified in the $Agl^{-/-}$ mice. Interestingly, we identified *ITGB4* (integrin subunit beta 4) and *GDF15* (growth differentiation factor 15). We validated increased expression of *Itgb4* and *Gdf15* by qPCR in $Agl^{+/+}$ and $Agl^{-/-}$ tumors (n = 8 per group; Figure 3D). Furthermore, we investigated if genes described previously to be associated with AGL (3) could be validated in our $Agl^{-/-}$ mice. Even though we observed gene expression changes matching the direction of previous observations (e.g. increased hyaluronic acid synthase 2 (HAS2) expression in AGL $Agl^{-/-}$ mice), the results were not statistically significant ($P > 0.05$). Both genes show significantly higher expression in patient tumor tissue compared with normal urothelium matching the observations made in the mice (Figure 3E and F). These data provide evidence that the observations in our mouse models have translational relevance to human disease.

Discussion

We and others have shown AGL is a suppressor of tumor growth in established tumor models (2,3,6). Herein, we sought to determine if AGL expression in normal tissues impacts their susceptibility to carcinogenesis. To investigate this question, we developed conventional germline and conditional bladder-specific AGL knockout murine models. Our germline $Agl^{-/-}$ knockout

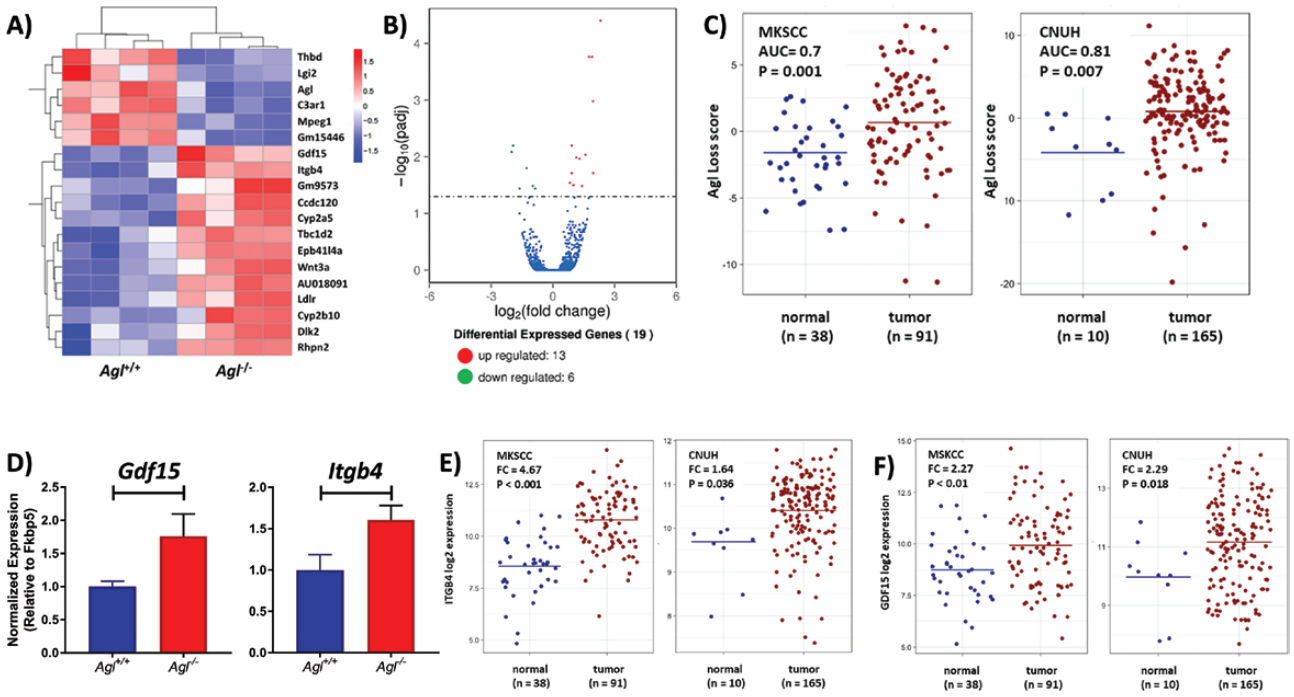

Figure 3. RNA-seq analysis of bladder tumors derived from $Agl^{-/-}$ and $Agl^{+/+}$ mice identifies a tumor-promoting gene set. RNA-seq was performed on $Agl^{+/+}$ ($n = 4$) and $Agl^{-/-}$ ($n = 4$) mice. (**A**) Unsupervised clustering of the eight tumors properly segregates tumors from $Agl^{+/+}$ and $Agl^{-/-}$ mice. (**B**) Volcano plot depicting the 19 significant (P-adj < 0.05) differentially expressed genes in $Agl^{-/-}$ mice compared with $Agl^{+/+}$ mice. (**C**) The '*Agl* Loss' score was defined from the 19 differentially expressed genes identified and used to determine if it could appropriately discriminate normal bladder urothelium and tumor tissue from patients from two independent and publicly available datasets. Two differentially expressed genes in the human dataset, (**D**) *Itgb4* and *Gdf15* were validated in $Agl^{-/-}$ and $Agl^{+/+}$ mouse tumors by qPCR. Additionally, (**E**) ITGB4 and (**F**) GDF15 have significantly higher levels in tumor tissue compared with normal tissue. Bars denote significant differences ($P < 0.05$).

model recapitulates previous findings of a murine GSDIII phenotype, confirming the validity of our model (14). Even though the observed increase in tumor incidence in our *Agl* KO models was not statistically significant, our data suggest that AGL has a role in bladder carcinogenesis, especially because the same result was obtained with mice having conditional knockout of *Agl* in bladder urothelium. However, the relative importance of AGL loss in driving carcinogenesis, and how this compares with AGL loss in driving established tumors, remains unclear (2,3).

Our work defined a novel '*Agl* Loss' gene signature composed of the 19 differentially expressed genes from RNA-seq of tumors resulting from BBN carcinogenesis. The *Agl* Loss score was able to stratify normal and BC tissue from publicly available datasets (21,22). These findings support the biological and clinical relevance of murine tumors derived from normal tissues lacking AGL. Interestingly, the 19 genes identified herein were not differentially expressed in our previously described model of shAGL (3). In the previously referenced experiments, established human BC cells were transduced with a shAGL construct to reduce AGL protein levels (3). The lack of similarity between the referenced shAGL experiments and those presented herein are not surprising for several reasons. The species used in the two studies were different. In the currently described murine experiments, normal urothelium-lacking AGL was transformed by chemical carcinogens. It is plausible that incomplete protein knockdown by shAGL lead to a different transcriptional profile than conventional germline *Agl* knockout in the mouse models described previously. We can also speculate that AGL loss prior to transformation can result in a different transcriptional program than AGL loss occurring during tumor progression. Despite the biological and technical differences between microarray and RNA-seq, evaluation of the top five genes identified in Guin *et al.* (3) revealed similar albeit nonstatistically significant relationships when comparing tumors with and without AGL expression. To begin to determine the reason for these differences, it would be of interest to develop BC cell lines from murine tumors of $Agl^{+/+}$, $Agl^{-/-}$, $Agl^{fl/fl}$ and $Agl^{fl/fl}$;*UpkII-Cre*$^{+/Tg}$ mice and transcriptionally profile them after knockout of *Agl* or reconstitution with a constitutively active *Agl*, as appropriate.

One of the 13 genes with increased expression in $Agl^{-/-}$ tumors was *Gdf15*. We found expression of *GDF15* is increased in human BC compared with normal tissue. GDF15 is a member of the transforming growth factor-beta (TGF-beta) superfamily first described as an inhibitor of macrophages (29). Interestingly, GDF15 is typically expressed at low levels in a majority of normal tissues but has high expression in liver (29). Coincidently, the primary organ impacted by the loss of AGL is liver (30). GDF15 upregulation in the context of BBN carcinogenesis is compatible with the inevitable inflammation caused by carcinogenic stimuli (31). Increased GDF15 expression has been associated with older age, male sex, smoking and obesity; all of which are known risk factors for BC (32). Although the full role of GDF15 remains to be determined, studies indicate GDF15 may have both tumor suppressor (33,34) and pro-tumorigenic (35,36) functions. This is not dissimilar to characteristics of other members of the transforming growth factor-beta superfamily, where their role is context dependent (37,38). Interestingly, GDF15 has been identified as a BC biomarker (39), with increased levels being associated with poor outcome (40).

Our transcriptomic analysis of $Agl^{-/-}$ tumors also identified *Itgb4* as being upregulated in $Agl^{-/-}$ tumors. Integrins are deeply implicated in tumor biology, and have been shown to play critical roles in metastasis and microenvironmental interactions (41). Increased ITGB4 has previously been associated with more aggressive BC and hepatocellular carcinoma phenotypes (42,43).

Increased tumor aggressiveness due to ITGB4 expression is associated with an induction of epithelial–mesenchymal transition, primarily through an upregulation of Slug (43). Our prior work has implicated the pro-tumorigenic properties of CD44, so it was interesting to observe other cell adhesion molecules, such as ITGB4, playing a role in mediating the aggressive phenotype conferred by AGL loss (5,6,44). Taken together, these observations suggest that AGL may be functioning through a shared pathway that leads to loss of contact inhibition and increased tumor growth. These alterations may also lead to increased metastasis because loss of cell adhesion molecules is a hallmark of the metastatic cascade (45,46).

The tumor microenvironment is well known to regulate tumor growth and impact tumor heterogeneity (31,47,48). Therefore, the development of a bladder urothelium-specific knockout of *Agl* is important for future studies as a BC model with clinical relevance. The conditional knockout model addresses a weakness of $Agl^{-/-}$ models, in that the gene of interest is only altered in the tissue of interest rather than the entire organism. For example, in the $Agl^{-/-}$ model, *Agl* is lost in hepatocytes, macrophages, neurons, endothelial cells and all other cells, which may impact aspects of carcinogenesis our model did not detect. However, the $Agl^{-/-}$ strain is useful to study cancer predisposition in patients with GSDIII. Indeed, our work suggests that GSDIII patients may have an increased susceptibility to BC development, and further investigation is necessary to determine if GSDIII patients should undergo increased screening for development of BC.

Finally, the concept of field cancerization, where widespread carcinogenic alterations occur in a large proportion of cells despite a lack of morphologic differentiation, is understood to contribute to the multifocal nature of BC development (49). Our findings support studies aimed at evaluating individuals at higher risk for BC (e.g. smokers) for reduced AGL expression in their urothelium. If smokers have decreased AGL expression compared with nonsmokers, these data would be supportive of the role AGL plays in BC carcinogenesis. Further, as not all smokers develop BC, individuals that smoke and have decreased AGL expression may be at an even higher risk for developing BC, and thus may be candidates for screening (50).

Funding

National Institute of Health Grant (CA143971 to D.T.); Italian Telethon (GGP15051 to G.P.C.).

Acknowledgements

We would like to thank Dr. Xue-Ru Wu for the generous gift of the $UpkII\text{-}Cre^{+/Tg}$ mice. We would like to thank EUCOMM for the ES cells and sperm used to develop the mouse models presented herein. We would also like to thank Dr. Linda K. Johnson at the University of Colorado–Anschutz Medical Campus and the Comparative Pathology core for her help in acquiring the histo-logic images presented herein.
Conflict of Interest Statement: None declared.

References

1. Siegel, R.L. *et al.* (2018) Cancer statistics, 2018. CA. Cancer J. Clin., 68, 7–30.
2. Guin, S. *et al.* (2014) Role in tumor growth of a glycogen debranching enzyme lost in glycogen storage disease. J Natl Cancer Inst., 106, dju062.
3. Guin, S. *et al.* (2016) Loss of glycogen debranching enzyme AGL drives bladder tumor growth via induction of hyaluronic acid synthesis. Clin. Cancer Res., 22, 1274–1283.
4. Bao, Y. *et al.* (1996) Human glycogen debranching enzyme gene (AGL): complete structural organization and characterization of the 5′ flanking region. Genomics, 38, 155–165.
5. Ahmed, M. *et al.* (2016) An osteopontin/CD44 axis in RhoGDI2-mediated metastasis suppression. Cancer Cell, 30, 432–443.
6. Oldenburg, D. *et al.* (2016) CD44 and RHAMM are essential for rapid growth of bladder cancer driven by loss of glycogen debranching enzyme (AGL). BMC Cancer, 16, 713.
7. Ritterson Lew, C. *et al.* (2015) Targeting glycogen metabolism in bladder cancer. Nat. Rev. Urol., 12, 383–391.
8. Talente, G.M. *et al.* (1994) Glycogen storage disease in adults. Ann. Intern. Med., 120, 218–226.
9. Pagliarani, S. *et al.* (2014) Glycogen storage disease type III: a novel Agl knockout mouse model. Biochim. Biophys. Acta, 1842, 2318–2328.
10. Haagsma, E.B. *et al.* (1997) Type IIIb glycogen storage disease associated with end-stage cirrhosis and hepatocellular carcinoma. The Liver Transplant Group. Hepatology, 25, 537–540.
11. Demo, E. *et al.* (2007) Glycogen storage disease type III-hepatocellular carcinoma a long-term complication? J. Hepatol., 46, 492–498.
12. Williams, P.D. *et al.* (2008) Molecular credentialing of rodent bladder carcinogenesis models. Neoplasia, 10, 838–846.
13. Ayala de la Peña, F. *et al.* (2011) Loss of p53 and acquisition of angiogenic microRNA profile are insufficient to facilitate progression of bladder urothelial carcinoma in situ to invasive carcinoma. J. Biol. Chem., 286, 20778–20787.
14. Liu, K.M. *et al.* (2014) Mouse model of glycogen storage disease type III. Mol. Genet. Metab., 111, 467–476.
15. Herz, J. *et al.* (1992) LDL receptor-related protein internalizes and degrades uPA-PAI-1 complexes and is essential for embryo implantation. Cell, 71, 411–421.
16. Mo, L. *et al.* (2005) Gene deletion in urothelium by specific expression of Cre recombinase. Am. J. Physiol. Renal Physiol., 289, F562–F568.
17. Zhang, Z.T. *et al.* (2001) Role of Ha-ras activation in superficial papillary pathway of urothelial tumor formation. Oncogene, 20, 1973–1980.
18. Cheng, J. *et al.* (2002) Overexpression of epidermal growth factor receptor in urothelium elicits urothelial hyperplasia and promotes bladder tumor growth. Cancer Res., 62, 4157–4163.
19. Akman, H.O. *et al.* (2011) Animal models of glycogen storage disorders. Prog. Mol. Biol. Transl. Sci., 100, 369–388.
20. Nelson, T.E. *et al.* (1970) A rapid micro assay method for amylo-1,6-glucosidase. Anal. Biochem., 33, 87–101.
21. Sanchez-Carbayo, M. *et al.* (2006) Defining molecular profiles of poor outcome in patients with invasive bladder cancer using oligonucleotide microarrays. J. Clin. Oncol., 24, 778–789.
22. Kim, W.J. *et al.* (2010) Predictive value of progression-related gene classifier in primary non-muscle invasive bladder cancer. Mol. Cancer, 9, 3.
23. Barrett, T. *et al.* (2013) NCBI GEO: archive for functional genomics data sets–update. Nucleic Acids Res., 41, D991–D995.
24. Miller, J.A. *et al.* (2011) Strategies for aggregating gene expression data: the collapseRows R function. BMC Bioinformatics, 12, 322.
25. Airoldi, L. *et al.* (1994) Detection of O6-butyl- and O6-(4-hydroxybutyl) guanine in urothelial and hepatic DNA of rats given the bladder carcinogen N-nitrosobutyl(4-hydroxybutyl)amine. Carcinogenesis, 15, 2297–2301.
26. Okada, M. *et al.* (1977) Metabolic fate of N-n-butyl-N-(4-hydroxybutyl)-nitrosamine and its analogues. Selective induction of urinary bladder tumours in the rat. Xenobiotica, 7, 11–24.
27. Kong, X.T. *et al.* (2004) Roles of uroplakins in plaque formation, umbrella cell enlargement, and urinary tract diseases. J. Cell Biol., 167, 1195–1204.
28. Moll, R. *et al.* (1995) Uroplakins, specific membrane proteins of urothelial umbrella cells, as histological markers of metastatic transitional cell carcinomas. Am. J. Pathol., 147, 1383–1397.

29. Bootcov, M.R. *et al.* (1997) MIC-1, a novel macrophage inhibitory cytokine, is a divergent member of the TGF-beta superfamily. Proc. Natl. Acad. Sci. U S A, 94, 11514–11519.
30. Hsiao, E.C. *et al.* (2000) Characterization of growth-differentiation factor 15, a transforming growth factor beta superfamily member induced following liver injury. Mol. Cell. Biol., 20, 3742–3751.
31. Sui, X. *et al.* (2017) Inflammatory microenvironment in the initiation and progression of bladder cancer. Oncotarget, 8, 93279–93294.
32. Mimeault, M. *et al.* (2010) Divergent molecular mechanisms underlying the pleiotropic functions of macrophage inhibitory cytokine-1 in cancer. J. Cell. Physiol., 224, 626–635.
33. Baek, S.J. *et al.* (2001) Cyclooxygenase inhibitors regulate the expression of a TGF-beta superfamily member that has proapoptotic and antitumorigenic activities. Mol. Pharmacol., 59, 901–908.
34. Tsui, K.H. *et al.* (2015) Growth differentiation factor-15: a p53- and demethylation-upregulating gene represses cell proliferation, invasion, and tumorigenesis in bladder carcinoma cells. Sci. Rep., 5, 12870.
35. Eling, T.E. *et al.* (2006) NSAID activated gene (NAG-1), a modulator of tumorigenesis. J. Biochem. Mol. Biol., 39, 649–655.
36. Nakamura, T. *et al.* (2003) Quantitative analysis of macrophage inhibitory cytokine-1 (MIC-1) gene expression in human prostatic tissues. Br. J. Cancer, 88, 1101–1104.
37. Gupta, S. *et al.* (2016) Transforming growth factor-β is an upstream regulator of mammalian target of rapamycin complex 2-dependent bladder cancer cell migration and invasion. Am. J. Pathol., 186, 1351–1360.
38. Massagué, J. (2008) TGFβ in cancer. Cell, 134, 215–230.
39. Costa, V.L. *et al.* (2010) Three epigenetic biomarkers, GDF15, TMEFF2, and VIM, accurately predict bladder cancer from DNA-based analyses of urine samples. Clin. Cancer Res., 16, 5842–5851.
40. Wallentin, L. *et al.* (2013) GDF-15 for prognostication of cardiovascular and cancer morbidity and mortality in men. PLoS One, 8, e78797.
41. Cohen, M.B. *et al.* (1997) Cellular adhesion molecules in urologic malignancies. Am. J. Clin. Pathol., 107, 56–63.
42. Grossman, H.B. *et al.* (2000) Expression of the alpha6beta4 integrin provides prognostic information in bladder cancer. Oncol. Rep., 7, 13–16.
43. Li, X.L. *et al.* (2017) Integrin β4 promotes cell invasion and epithelial-mesenchymal transition through the modulation of Slug expression in hepatocellular carcinoma. Sci. Rep., 7, 40464.
44. Sottnik, J.L. *et al.* (2016) CD44: a metastasis driver and therapeutic target. Oncoscience, 3, 320–321.
45. Bierie, B. *et al.* (2017) Integrin-β4 identifies cancer stem cell-enriched populations of partially mesenchymal carcinoma cells. Proc. Natl. Acad. Sci. U S A, 114, E2337–E2346.
46. Seguin, L. *et al.* (2015) Integrins and cancer: regulators of cancer stemness, metastasis, and drug resistance. Trends Cell Biol., 25, 234–240.
47. Marciscano, A.E. *et al.* (2018) Targeting the tumor microenvironment with immunotherapy for genitourinary malignancies. Curr. Treat. Options Oncol., 19, 16.
48. Routy, B. *et al.* (2018) Gut microbiome influences efficacy of PD-1-based immunotherapy against epithelial tumors. Science, 359, 91–97.
49. Curtius, K. *et al.* (2018) An evolutionary perspective on field cancerization. Nat. Rev. Cancer, 18, 19–32.
50. Starke, N. *et al.* (2016) Long-term outcomes in a high-risk bladder cancer screening cohort. BJU Int., 117, 611–617.